# Simulation and Analysis of Image Data from Crossed Beam Experiments

**George C. McBane**

**Department of Chemistry, The Ohio State University, Columbus, OH 43210**

Simulation of images expected from velocity mapping of crossed molecular beams is described. A general expression for the expected image is derived. Simplifying approximations and methods of forward convolution fitting are discussed. The analysis of a state to state experiment on Ne–CO rotationally inelastic scattering is shown as an example.

## Introduction

In a traditional crossed molecular beam experiment (*1*), a detector with a small aperture is located far away from the intersection volume of two collimated beams. Most molecules scattered from the intersection do not move toward the detector, and are lost. Such molecules represent an opportunity for improved experimental design; if they could be detected without sacrificing the angular information provided by the small-angular-acceptance detectors, the signal collection rate could be increased enormously. The potential advantages of ion imaging (discussed extensively in this volume) to crossed beam experiments have been apparent at least since its first application to photodissociation (*2*). In an ion imaging experiment, products scattered into all directions are photoionized in the intersection volume. Electrostatic fields then direct all the ions onto a position sensitive detector; the arrival positions of the ions provide information about the velocity vectors of the original scattered molecules.

Applications of ion imaging to crossed beam experiments have been slow in coming. The first example was provided by Bontuyan et al. (*3*), who studied Ar + NO inelastic scattering with 1+1 resonance enhanced ionization of NO; further work on the same system was reported by Yonekura et al. (*4*). The H + $H_2$ reaction was investigated by Kitsopolous et al. (*5*). Peterka et al. studied the O($^1D$) + $D_2$ reaction (*6*). Several more papers are in press (*7–10*).

## The Idealized Experiment

In an ideal crossed beam experiment with ion imaging detection, two molecular beams with sharp velocities and no angular divergence would intersect. Scattered product molecules would then be photoionized with an efficiency independent of their positions and velocities. The ions would be propelled by external electric fields (and not repelled by one another!) onto a detector in a way that permitted the postcollision velocity vector of each arriving ion to be determined accurately. In the simplest case, the undetected sibling products would have only one accessible internal state.

Under these circumstances, the two-dimensional distribution of intensities appearing on the detector may be directly interpreted to give the differential cross section (DCS) for scattering. If the relation between initial velocity and ion arrival position is a simple projection of the velocity vector onto the plane of the detector, and the detector plane is parallel to the initial relative velocity vector, the resulting ion image will be a disk with a sharp edge. The brightness of the disk in any annulus about its center, as a function of angular displacement from the initial relative velocity vector, gives the DCS.

No real experiment duplicates these ideal conditions. Real experiments have finite velocity distributions in the molecular beams, nonuniform photoionization probabilities, and imperfect correlations between ion arrival positions and velocities of scattered molecules. They may also be complicated by internal state distributions of undetected products. This article describes the effects of these nonidealities, their incorporation into realistic simulations of experiments, and useful ways of analyzing data in their presence.

## Real Experiments: Simulation

In photodissociation experiments, it is not too difficult to realize the equivalent of the "ideal experiment" described above. If the photolysis volume is small, the detection volume is large, and Doppler selectivity in the photoionization and space charge effects are negligible, then the ion image of photodissociation products can be inverted directly to give the speed and angular distribution of the products. The inverse Abel transform widely used in imaging studies of photodissociation is an example of such a direct inversion (*11*).

In the crossed beam case, even with sharp velocity distributions in the beams, the Abel transform is not usually available. The pulsed molecular beams used in the experiments have durations long compared to the flight times of scattered molecules across the detection volume. Molecules moving along the probe laser beam can be formed rather early in the molecular beam pulse and still be detected, while molecules formed that early but moving perpendicular to the probe laser will not be detected. The cylindrical symmetry present in the COM-frame velocity vector distribution is consequently not retained in the distribution of ions produced by the probe laser. The inverse Abel transform, which requires this symmetry, is therefore not valid. Other direct methods might still work in this case, but finite velocity spreads in the molecular beams add

an additional averaging that removes the rigorous validity of any direct deconvolution method. Experimenters are left with two choices: assume (incorrectly) the absence of velocity spreads, apply a direct method, and try to assess the importance of the resulting errors; or use a fitting procedure that incorporates the experimental averages. The latter approach has been widely used in traditional time of flight crossed beam studies. The next sections develop the corresponding analysis for ion imaging of crossed beam products.

### General Expression for Observed Intensity Distribution

The data in an ion imaging experiment are the intensities in the pixels of an image. Each pixel covers a small part, usually rectangular, of the two-dimensional detector. This description is useful whether the data were collected directly as pixel intensities in an "analog" mode or were obtained by digitizing individual ion arrival positions and then histogramming them into a 2D image (*12*).

In collisions with well defined relative velocity $g = |\mathbf{v}_1 - \mathbf{v}_2|$, the density of products scattered per unit time from initial state $i$ to final state $f$ into center of mass (COM) scattering angles $\theta$ and $\phi$ is

$$\frac{dn_{\mathrm{p}}(\theta, \phi, i \rightarrow f)}{dt} = \frac{d\sigma}{d\omega}(\theta, \phi, g, i \rightarrow f) g n_1 n_2, \tag{1}$$

where $\frac{d\sigma}{d\omega}$ is the state to state differential cross section and $n_1$ and $n_2$ are the densities of beams 1 and 2 at the intersection point. The state label $i \rightarrow f$ will be suppressed in further expressions; experiments that are not state to state will require an additional average over initial states and sum over final states in the equations below.

In most crossed beam experiments with pulsed laser detection, the molecular beams are also pulsed; then, $n_1$ and $n_2$ are distributions in position, velocity, and time. The signal depends on the density distribution of products at the time the probe laser fires, called $t = 0$; times before the probe are negative. A molecule scattered at position $\mathbf{r}_{\mathrm{s}}$ with laboratory-frame velocity $\mathbf{v}$ at time $t$ ($< 0$) will be at position $\mathbf{r}_{\mathrm{s}} - \mathbf{v}t$ at $t = 0$. The velocity $\mathbf{v}$ is a function of the initial velocity vectors of the colliding reactants $\mathbf{v}_1$ and $\mathbf{v}_2$, and the scattering angles $\theta$ and $\phi$. To find the product densities at $t = 0$, one adds all the contributions from earlier scattering times and positions of molecules that could contribute to the density at $\mathbf{r}$ at $t = 0$:

$$\begin{aligned} n_{\mathrm{p}}(\theta, \phi, \mathbf{r}, \mathbf{v}_1, \mathbf{v}_2, t = 0) &= \int_{-\infty}^{0} dt \int d\mathbf{r}_{\mathrm{s}} \frac{d\sigma}{d\omega}(\theta, \phi, g) g n_1(\mathbf{v}_1, \mathbf{r}_{\mathrm{s}}, t) n_2(\mathbf{v}_2, \mathbf{r}_{\mathrm{s}}, t) \\ &\quad \times \delta(\mathbf{r} - (\mathbf{r}_{\mathrm{s}} - \mathbf{v}t)) \\ &= \int_{-\infty}^{0} dt \, \frac{d\sigma}{d\omega}(\theta, \phi, g) g n_1(\mathbf{v}_1, \mathbf{r} + \mathbf{v}t, t) n_2(\mathbf{v}_2, \mathbf{r} + \mathbf{v}t, t) \end{aligned} \tag{2}$$

The distribution of product *ions* is given by the density of product molecules times the ionization probability $P_\mathrm{I}$, which is a function of both the position (through the spatial dependence of the laser intensity) and the velocity (through the Doppler shift). ($P_\mathrm{I}$ probably also depends on $f$, the final state of the molecule, because of different absorption probabilities for different final states.) The number of product ions with a particular $\theta$ and $\phi$, produced by scattering from beams with initial velocities $\mathbf{v}_1$ and $\mathbf{v}_2$ is

$$N_\mathrm{I}(\theta, \phi, \mathbf{v}_1, \mathbf{v}_2) = \int_V d\mathbf{r}\, n_\mathrm{p}(\theta, \phi, \mathbf{r}, \mathbf{v}_1, \mathbf{v}_2, t = 0) P_\mathrm{I}(\mathbf{r}, \mathbf{v}), \tag{3}$$

where the integration over $\mathbf{r}$ must include both the molecular beam intersection volume and the volume from which ions can be collected and sent toward the detector. The total number of product ions with COM scattering angles $\theta$ and $\phi$ is found by integrating over the velocity distributions in the two molecular beams:

$$\begin{aligned} N_\mathrm{I}(\theta, \phi) &= \int d\mathbf{v}_1 \int d\mathbf{v}_2\, N_\mathrm{I}(\theta, \phi, \mathbf{v}_1, \mathbf{v}_2) \\ &= \int d\mathbf{v}_1 \int d\mathbf{v}_2 \int_V d\mathbf{r} \int_{-\infty}^{0} dt\, \frac{d\sigma}{d\omega}(\theta, \phi, g) g \\ &\quad \times n_1(\mathbf{v}_1, \mathbf{r} + \mathbf{v}t, t) n_2(\mathbf{v}_2, \mathbf{r} + \mathbf{v}t, t) P_\mathrm{I}(\mathbf{r}, \mathbf{v}) \end{aligned} \tag{4}$$

In a velocity mapped imaging experiment, the observed quantity is the number of ions arriving in a particular pixel. If the velocity mapping optics are perfect, the arrival positions of the ions depend only on their velocity components in the detector plane (that is, perpendicular to the time of flight axis). To find the pixel intensities one must transform Eq. (4) to Cartesian velocity coordinates ($v_x$ and $v_y$). The transformation to Cartesian coordinates inserts a Jacobian that has a very simple form: it is proportional to $1/|v_z|$, the reciprocal of the velocity component along the time of flight axis. For each $\mathbf{v}_1, \mathbf{v}_2$ pair, there are at most two values of $v_z$ that contribute to the signal at a particular $(v_x, v_y)$, one from the "upper half" of the Newton sphere and one from the lower half. (If the velocity projection $(v_x, v_y)$ lies outside the Newton sphere, no ions will arrive there; if it lies exactly at the edge of the Newton sphere, there is only one $\mathbf{v}$ that will contribute, namely $(v_x, v_y, 0)$.) The two contributions simply add, and the intensity in a single pixel is obtained by integrating over its surface. Then

$$\begin{aligned} N_\mathrm{I}(v_x, v_y) = \int_{\Delta v_x} dv_x \int_{\Delta v_y} dv_y \int d\mathbf{v}_1 \int d\mathbf{v}_2 \int_V d\mathbf{r} \int_{-\infty}^{0} dt\, g \left| \frac{\partial\theta\, \partial\phi}{\partial v_x \partial v_y} \right| \\ \times \left[ \frac{d\sigma}{d\omega}(\theta^+, \phi^+, g) n_1(\mathbf{v}_1, \mathbf{r} + \mathbf{v}^+ t, t) n_2(\mathbf{v}_2, \mathbf{r} + \mathbf{v}^+ t, t) P_\mathrm{I}(\mathbf{r}, \mathbf{v}^+) \right. \\ \left. + \frac{d\sigma}{d\omega}(\theta^-, \phi^-, g) n_1(\mathbf{v}_1, \mathbf{r} + \mathbf{v}^- t, t) n_2(\mathbf{v}_2, \mathbf{r} + \mathbf{v}^- t, t) P_\mathrm{I}(\mathbf{r}, \mathbf{v}^-) \right], \end{aligned} \tag{5}$$

where $\mathbf{v}^+$ and $\mathbf{v}^-$ are the "upper half" and "lower half" velocity vectors. The $x$ and $y$ components of $\mathbf{v}^+$ and $\mathbf{v}^-$ are the same; their $z$ components will be equal in magnitude but opposite in sign if the COM velocity is perpendicular to the TOF axis. $\theta^+$ amd $\phi^+$ are the upper-half COM scattering angles; $\theta^+ = \theta^-$ if the relative velocity is perpendicular to the TOF axis.

If the velocity mapping optics are not perfect, then the arrival position of an ion may depend on both its velocity $\mathbf{v}$ and its position of formation $\mathbf{r}$. An explicit projection procedure is then required to reduce the five variables $\theta$, $\phi$, and $\mathbf{r}$ to the detector position variables $x_d$ and $y_d$. The projection is straightforward if the function giving $x_d$ and $y_d$ in terms of $\theta$, $\phi$, and $\mathbf{r}$ is known.

Equation 5 is a general expression for the final two-dimensional velocity distribution in terms of the differential cross section and quantities determined by the apparatus. It may be compared to the similar expression given by Buck for a more traditional crossed beam apparatus with a detector located far from the scattering center, eq (18.23) of Ref. 13. There are several minor differences, but the Jacobian is quite different in the two cases. In the traditional experiment the COM solid angle subtended by the detector varies strongly as the laboratory scattering angle changes. In the imaging experiment the COM solid angles vary simply with the distance of the pixel away from the COM velocity; the strong variation of angular resolution with scattering angle characteristic of the traditional experiment is no longer present.

**Simplifying Approximations**

Equation 5 is a twelve-dimensional integral. Most programs that simulate images from crossed beam experiments make approximations that reduce its dimensionality before attempting the integration. This section describes the approach followed in my own simulations of CO scattering experiments; it is similar to that used by several other groups.

In the crossed beam imaging apparatus at Sandia, the two molecular beams are very tightly collimated, with half-angles of 0.23°, and cross at right angles. Their speed ratios are modest ($S$ = 15–20). Under these circumstances the distributions of relative velocities $\mathbf{v}_1 - \mathbf{v}_2$ and of COM velocity vectors $\mathbf{v}_{COM}$ are almost entirely determined by the spread in speeds of the two molecular beams rather than their angular spreads. We can therefore reduce the six-dimensional integral over the molecular beam velocities $\mathbf{v}_1$ and $\mathbf{v}_2$ to a two-dimensional one over their magnitudes alone. This reduction is not usually available; in experiments with looser collimation the angular spread of the beams will make important contributions to the distribution of COM and relative velocities (*14*).

A second approximation is that the pixels are sufficiently small that only the Jacobian from Eq. (5) varies significantly over the small region defined by $\Delta v_x$, $\Delta v_y$. All the other quantities can be evaluated at the values of $v_x$ and $v_y$ that describe the center of the pixel. This approximation is reasonable if features in the experimental images are large compared to single pixels.

With these two approximations Eq. (5) reduces to

$$N_{\mathrm{I}}(\bar{v}_x, \bar{v}_y) = \int dv_1 \int dv_2 \, g\bar{J}(v_1, v_2, \bar{v}_x, \bar{v}_y) \times \left[ \frac{d\sigma}{d\omega}(\bar{\theta}^+, \bar{\phi}^+, g) F(v_1, v_2, \mathbf{v}^+) + \frac{d\sigma}{d\omega}(\bar{\theta}^-, \bar{\phi}^-, g) F(v_1, v_2, \mathbf{v}^-) \right] \quad (6)$$

where the barred variables represent quantities evaluated at the center of a particular pixel, and

$$\bar{J}(v_1, v_2, \bar{v}_x, \bar{v}_y) = \int_{\bar{v}_x - \Delta v_x}^{\bar{v}_x + \Delta v_x} dv_x \int_{\bar{v}_y - \Delta v_y}^{\bar{v}_y + \Delta v_y} dv_x \left| \frac{\partial\theta \, \partial\phi}{\partial v_x \partial v_y} \right| \quad (7)$$

$$F(v_1, v_2, \mathbf{v}) = \int_V d\mathbf{r} \int_{-\infty}^{0} dt \, n_1(v_1, \mathbf{r} + \mathbf{v}t, t) n_2(v_2, \mathbf{r} + \mathbf{v}t, t) P_{\mathrm{I}}(\mathbf{r}, \mathbf{v}). \quad (8)$$

Eq 6 is simple enough to evaluate in practical programs. Either Monte Carlo or deterministic (e.g., nested Gaussian quadrature) methods may be used.

## Implementation

This section describes a particular program, called Imsim, that evaluates Eq. (6) and has been used in extraction of state to state differential cross sections for Ne–CO rotationally inelastic scattering.

Evaluation of Eq. (6) requires specification of the functions $n_1$, $n_2$, $P_{\mathrm{I}}$, $\frac{d\sigma}{d\omega}$, and $\left|\frac{\partial\theta \, \partial\phi}{\partial v_x \partial v_y}\right|$. In the Imsim program the molecular beam densities are assumed to have Gaussian profiles in the radial spatial dimension, in time (though with a temporal peak that might not fall at $t = 0$), and in speed. The ionization probability is proportional to the intensity of a focused Gaussian laser beam at the Doppler-shifted absorption frequency $\nu_{\mathrm{abs}}$ and at the position $\mathbf{r}$, raised to a power given by the number of photons in the absorption. The Jacobian in the perfect velocity mapping case is

$$\left| \frac{\partial\theta \, \partial\phi}{\partial v_x \partial v_y} \right| = \frac{2}{|\mathbf{u}_f|^2 (|\mathbf{u}_f|^2 - u_x^2 - u_y^2)^{\frac{1}{2}}}, \quad (9)$$

where $\mathbf{u}_f$ is the final velocity in the COM frame, and $u_x$ and $u_y$ are its components in the plane perpendicular to the TOF direction. A user-supplied function evaluates the differential cross section so any reasonable shape can be used.

The outer integration over $v_1$ and $v_2$ is performed with trapezoidal rule quadrature, using typically 30 speeds for each beam. The Jacobian integral is expressed analytically (*15*) and evaluated for each pixel at each $v_1/v_2$ pair. The integrand of the three-dimensional integral over space is very strongly peaked if the laser beam is tightly

focused. In Imsim this integral is performed with Gaussian quadratures that incorporate all the spatial dependence of the laser intensity into the Gaussian weighting functions (*16*, *17*), so that relatively few spatial quadrature points are required (125 points at each $t$ is typical). The integral over time is performed with Gauss-Legendre quadrature; a finite lower integration limit is chosen for each pixel so that scattering at earlier times contributes negligibly to the signal.

As just described, an accurate image simulation requires on the order of $10^6$ evaluations of the integrand (primarily the product of molecular beam densities) for each pixel; a typical image might be $100\times100$ pixels for a total of $10^{10}$ integrand evaluations. These evaluations will dominate the computation time. If each evaluation requires 100 floating point operations, then on a 100 MFLOPS computer the simulation will take about three hours.

If the molecular beam densities have the same speed distribution for every position and time, that is, if $n(v, \mathbf{r} + \mathbf{v}t, t) = s(v)\rho(\mathbf{r} + \mathbf{v}t, t)$, the simulation time can be reduced enormously by a simple trick. The speed distribution $s$ may be removed from the four-dimensional integration in the definition of $F$. For a specified pixel, the only remaining effect of $v_1$ and $v_2$ within the integral is to determine the position and diameter of the Newton sphere and therefore the $z$-component of $\mathbf{v}$. The four-dimensional integral over $\mathbf{r}$ and $t$ for a single pixel may then be regarded as a function of a single parameter, $v_z$. If the integral is determined accurately for a representative set of $v_z$ at each pixel, its value for other nearby $v_z$ (implying other values of $v_1$ and $v_2$) can be determined by interpolation. The integral is a smooth function of $v_z$, so that six representative $v_z$ support an accurate cubic spline interpolation. The number of 4D integral evaluations per pixel has then been reduced from 900 (for 30 speeds in each molecular beam) to six, with a corresponding reduction in run time. Typical simulations with Imsim using this trick require about five minutes; the run time is dominated by evaluations of $\bar{J}$.

## Real Experiments: Data Analysis

### Qualitative Analysis

One of the main attractions of imaging experiments is that the appearance of the image data immediately suggests simple qualitative interpretations. For instance, in rotationally inelastic scattering, the positions of rotational rainbow peaks are usually immediately apparent, and their changes in a series of images corresponding to different $\Delta j$ can be followed easily. In the most common geometry, with the TOF axis perpendicular to the molecular beam plane, each position on the outer edge of the Newton circle in the image corresponds roughly to a single scattering angle. The positions (though not the relative intensities) of sharp features in the DCS, and its overall shape, can usually be estimated directly from the image with an angular accuracy of $10^\circ$ or better. For qualitative interpretation this is sometimes all that is required.

A crude estimate of the DCS may be obtained by simply measuring the intensity near the edge of the image as a function of angular displacement about the COM velocity from the initial product velocity. This estimate is accurate if the detection

probabilities of all scattered molecules are the same. Most experiments do not meet that condition, and the resulting errors in intensities in the DCS can be large. (The corresponding requirement is easy to meet in photodissociation experiments, so that an equivalent analysis of photodissociation data is often reasonable.)

A better estimate may be obtained by performing a simulation for an *isotropic* DCS, then dividing that image into the observed image pixel by pixel. In the absence of velocity spreads in the two molecular beams, the quotient image would show a series of stripes of constant intensity perpendicular to the relative velocity vector. The pixel values in the stripes would give the DCS at the corresponding values of $\cos\theta$. The unique mapping between $\theta$ and pixel position is destroyed by the velocity spreads, but this method will still provide an initial estimate of the DCS that is better than that from a direct interpretation of uncorrected pixel intensities.

**Linear Fitting**

Integration is a linear operation. If the DCS in Eq. (6) is written as a linear combination of basis functions, a set of basis images may be obtained by performing simulations using each basis function as the DCS. Then the predicted image for any linear combination of basis functions is the corresponding linear combination of basis images. Narrow functions in angle space make good basis functions; Gaussians, triangles, and rectangles could all be used. Once the basis images have been generated, no further multidimensional integrals are required, and the simulated image for each new set of weighting coefficients can be assembled in milliseconds rather than minutes.

If the experiment does not resolve $m_j$ states so that the DCS has no $\phi$ dependence, and the desired quantity is the DCS averaged over the experimental distribution of relative speeds $g$, then the desired function $d\sigma/d\omega$ is a function of $\theta$ alone. If everything in Eq. (6) except the DCS is known, then its extraction from the data (i.e., determination of the optimum set of weighting coefficients in the DCS expansion) is a linear fitting problem. The data do not always determine the DCS at every angle very well, so it is usually an ill-conditioned problem. Methods from the field of inverse problems are needed to bias the result toward physically reasonable values in some regions. "By-hand" fitting, Tikhonov regularization (*18*), and van Cittert iteration (*19*) have all been used.

**Nonlinear Fitting**

If quantities other than the differential cross section—for example, the wavelength offset of the laser or the detector location and orientation—need to be fit to the data rather than specified in advance, then the problem is no longer a linear one. Iterative, rather than direct, methods must be applied. A program that uses a nonlinear optimization algorithm to adjust the few nonlinear parameters in an outer loop, with a simulation, a linear DCS fit, and computation of the resulting $\chi^2$ in its function-evaluation routine, often works well.

In some nonlinear problems, it is possible to generate new basis functions at each iteration without new simulations. When this kind of basis-image construction is available it is usually much faster than performing new simulations for each set of trial nonlinear parameters. For example, if the absolute wavelength of the probe laser is unknown, its value might be a nonlinear fitting parameter. If the laser beam is parallel to the detector, and velocity mapping is used, each pixel corresponds to a known velocity component along the laser beam. Corrections for Doppler weighting can therefore be applied to each basis image by multiplying a Doppler weighting function pixel by pixel into the basis images.

Other experimental parameters that often need to be fit are the orientation and position of the detector and the velocity-to-detector-position mapping factor (the effective flight time). These quantities specify the relation between laboratory frame velocity $(\bar{v}_x, \bar{v}_y)$ and pixel position in the image. It is reasonable to compute $N_I(\bar{v}_x, \bar{v}_y)$ at a suitably fine grid of $(\bar{v}_x, \bar{v}_y)$ points, then interpolate in that 2D grid to obtain simulated images for new values of detector position and effective flight time. This interpolation scheme again permits the parameters to be fit without new simulations at each iteration. It was used in the analysis of Ne–CO scattering data described next.

## Example: Analysis of Ne + CO Inelastic Scattering

The left panel of Figure 1 shows an experimental image obtained by 2+1 REMPI of scattered CO in a crossed beam Ne + CO experiment with velocity mapping. This image was obtained at Sandia National Laboratory; a detailed description of the apparatus and experimental procedures will be published elsewhere (*8*). The two molecular beams crossed at right angles; the probe laser traveled in the same plane and bisected the two oncoming molecular beams. Molecules scattered into $j_f = 10$ were ionized and the ions were accelerated perpendicular to the beam plane by velocity mapping optics. The initial CO rotational temperature was about 2 K. The speeds of the CO and Ne beams were 560 and 785 m/s, respectively, for a collision energy of 456 $cm^{-1}$. The 215 nm laser beam was focused at the molecular beam crossing point by a 0.5 m lens and was linearly polarized in the molecular beam plane.

The center panel of Figure 1 shows a simulated image with an isotropic DCS and other parameters chosen to represent the experiment. This image demonstrates the importance of the "kernel functions" that multiply the DCS in Eq. (5). The Jacobian causes the bright outer ring and dimmer center of the image; the velocity spread in the beams produces the fuzziness at the outer edge, which is more pronounced at the bottom of the image; the ionization probability and integration over time produce the bright spot near the top of the image and the slight weighting in a vertical stripe through the center. A naive analysis that simply used the intensity as a function of angle about the center as an estimate of the DCS would give very poor results, especially if the measurements were made around the upper edge of the image.

The right panel of Figure 1 shows a simulated image obtained from a nonlinear fit. The DCS was modeled as a piecewise linear function with values defined at 5° intervals; the basis functions were therefore narrow triangles. A set of basis images was

generated by simulation using no Doppler weighting and estimates of the other experimental parameters. A least squares fit was then performed; the wavelength offset of the laser, the detector position and orientation, and the effective flight time were varied in a nonlinear fitting loop. At each iteration, a new set of basis images was determined by interpolation, weightings for the Doppler effect were applied, and a linear fit of the DCS alone was performed with first order regularization. The best fit yielded detector position and effective flight time values that differed by less than 5% from the initial estimates. Figure 2 shows several 1D profiles through the data and best-fit images. Figure 3 shows the extracted DCS.

All the major features of the experimental image have been captured, but systematic disagreements between the fitted image and the data remain. Some of these disagreements come from imperfections in the velocity mapping; in particular, there appear to be some space charge effects in the bright spot at the top of the experimental image, the experimental image is blurrier than the simulation, and the main ring is not quite round. Angular momentum polarization was neglected during this fit. The effects of angular momentum polarization of the scattered molecules will be discussed briefly below.

## Further Applications

This section examines two points that were hidden in the discussion above by the assumption of complete initial and final quantum state resolution. One is the effect of angular momentum polarization on the images. The second is the possibility of unresolved internal energy distributions in the unprobed product.

### Polarization Effects

Scattered molecules with a given $j$ will usually have nonisotropic distributions of their angular momentum vectors. Laser ionization probes are sensitive to the angular momentum distribution, so if the molecules arriving in different pixels have different angular momentum distributions the relative pixel intensities will be affected. This dependence is both a nuisance and an opportunity; it must be accounted for even if one simply wants to measure a degeneracy averaged differential cross section, but it provides a rich source of dynamical information beyond the DCS if it can be exploited well.

It is straightfoward to include the effects of any known angular momentum polarization in simulations. Formulas cited in the excellent review by Orr-Ewing and Zare (*20*) may be incorporated easily into the $P_1$. On the other hand, the problem of extracting an unknown angular momentum distribution from images measured with different polarizations or geometries has not yet been fully addressed for the crossed-beam problem.

The Ne-CO analysis described above assumed that the scattered molecules were not polarized. One way to estimate the likely error introduced by that assumption is to perform additional fits assuming limiting nonisotropic polarizations, and see how

much the extracted DCS changes. In the present example, three fits were performed: one assuming no polarization, one assuming limiting positive alignment ($m_j = j$ and $m_j = -j$ equally populated, with all other $m_j$ unpopulated; the quantization vector is taken along the final COM frame velocity vector of the CO), and one assuming limiting negative alignment (only $m_j = 0$ populated). The most likely actual outcome of the scattering process is modest negative alignment. For the geometry of the experiment, negative alignment tends to enhance the intensity at extreme forward and backward scattering, while not affecting sideways scattering. Since this DCS does not have much intensity near the poles, the neglect of polarization effects does not introduce significant error.

### Unresolved Internal Energy Distributions

If the unprobed collider has accessible internal energy states, then the observed image will be a superposition of different images corresponding to different Newton sphere diameters. The object of the data analysis (discounting the distribution of collision energies) would be the two-dimensional energy-angle distribution. In photodissociation experiments this distribution is usually obtained with an inverse Abel transform. Suits et al. have applied this analysis to one crossed-beam study of the $O(^1D)$ + $D_2$ reaction (*6*); they used a very short oxygen atom beam and a loosely focused probe laser to reduce selective detection effects. In cases where the selective detection effects are stronger, one can imagine an extraction procedure in the spirit of the Abel transform: analyze the outermost ring, using only the data at the edge; simulate an image with the resulting DCS; subtract that image from the data, leaving a residual image with a smaller diameter, and work inwards. In such a procedure, small errors will propagate inward and grow, so the results will get steadily worse at higher internal energies. A general solution to this problem is not yet known.

## Acknowlegements

K. Thomas Lorenz and David W. Chandler acquired the experimental data with Department of Energy support. The author has benefited from conversations with David Chandler, Thomas Lorenz, Gregory Hall, and Michael Westley. Michael Westley provided the analytic Jacobian integral code.

## References

[1] Scoles, G., Ed.; *Atomic and Molecular Beam Methods;* Oxford University Press: New York, 1988.

[2] Chandler, D. W.; Houston, P. L. *J. Chem. Phys.* **1987,** *87,* 1445.

[3] Bontuyan, L. S.; Suits, A. G.; Houston, P. L.; Whitaker, B. J. *J. Phys. Chem.* **1993,** *97,* 6342–6350.

[4] Yonekura, N.; Gebauer, C.; Kohguchi, H.; Suzuki, T. *Rev. Sci. Inst.* **1999,** *70,* 3265–3270.

[5] Kitsopoulos, T. N.; Buntine, M. A.; Baldwin, D. P.; Zare, R. N.; Chandler, D. W. *Science* **1993,** *260,* 1605–1610.

[6] Ahmed, M.; Peterka, D. S.; Suits, A. G. *Chem. Phys. Lett.* **1999,** *301,* 372–378.

[7] Lorenz, K. T.; Westley, M. S.; Chandler, D. W. *Phys. Chem. Chem. Phys.* **2000,** submitted.

[8] Lorenz, K. T.; Chandler, D. W.; McBane, G. C. in preparation.

[9] Ahmed, M.; Peterka, D. S.; Suits, A. G. *Phys. Chem. Chem. Phys.* **2000,** in press.

[10] Ahmed, M.; Peterka, D. S.; Suits, A. G. *Chem. Phys. Lett.* **2000,** in press.

[11] Heck, A. J. R.; Chandler, D. W. *Annu. Rev. Phys. Chem.* **1995,** *46,* 335–372.

[12] Chang, B.-Y.; Hoetzlein, R. C.; Mueller, J. A.; Geiser, J. D.; Houston, P. L. *Rev. Sci. Inst.* **1998,** *69,* 1665–1670.

[13] Buck, U. General Principles and Methods. In *Atomic and Molecular Beam Methods*, Vol. I; Scoles, G., Ed.; Oxford University Press: New York, 1988.

[14] Buck, U. Elastic Scattering II. Differential Cross Sections. In *Atomic and Molecular Beam Methods*, Vol. I; Scoles, G., Ed.; Oxford University Press: New York, 1988.

[15] Westley, M. S. private communication.

[16] Gautschi, W. *ACM Trans. Math. Soft.* **1994,** *20,* 21–62.

[17] Elhay, S.; Kautsky, J. *ACM Trans. Math. Soft.* **1987,** *13,* 399–415.

[18] Press, W. H.; Teukolsky, S. A.; Vetterling, W. T.; Flannery, B. P. Numerical Recipes in C: the Art of Scientific Computing. In , second ed.; Cambridge University Press: New York, 1992; Chapter 18.

[19] Shapiro, M.; Gerber, R. B.; Buck, U.; Schleusener, J. *J. Chem. Phys.* **1977,** *67,* 3570–3576.

[20] Orr-Ewing, A. J.; Zare, R. N. *Ann. Rev. Phys. Chem.* **1994,** *45,* 315–366.

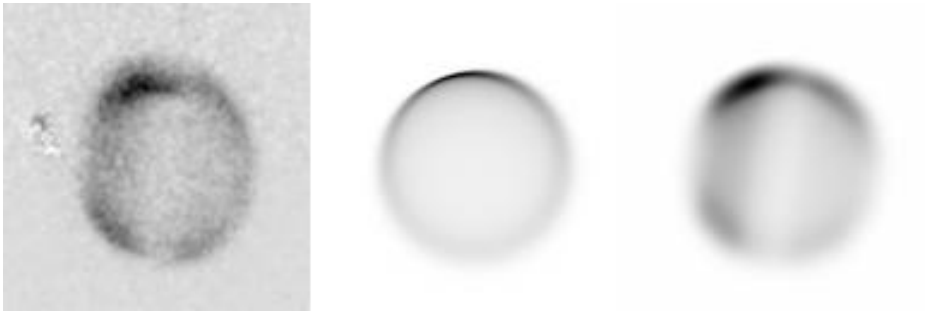

Figure 1: Left panel: experimental image for $j_f = 10$. Center panel: simulated image for isotropic differential cross section. Right panel: fitted image.

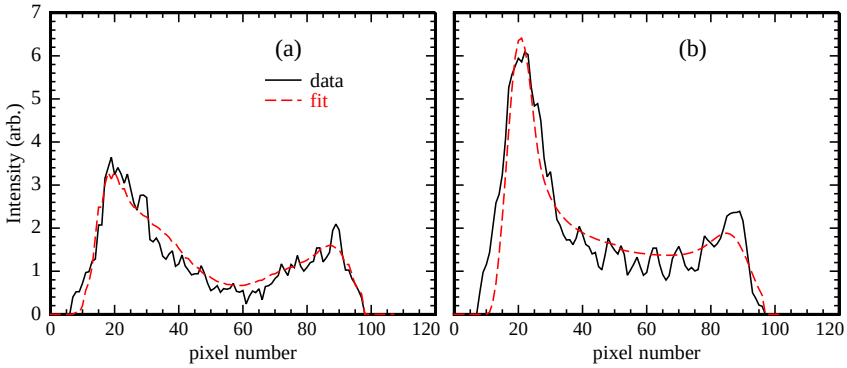


Figure 2: Line profiles through data and best-fit images. (a) diagonal trace from upper left to lower right of image; (b) vertical trace at column 54 (through brightest part of image).

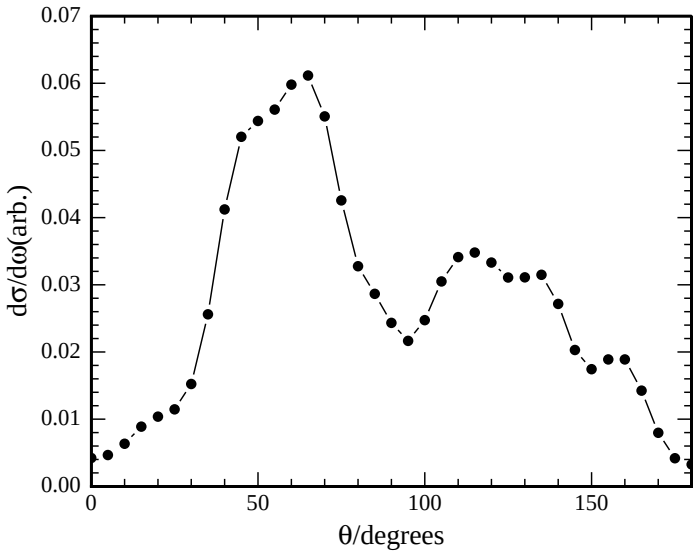


Figure 3: Fitted differential cross section.